Interface dynamics of strongly interacting binary superfluids

Yu-Ping An,[1,2,*] Li Li,[1,2,3,4,†] Chuan-Yin Xia,[5,6,‡] and Hua-Bi Zeng[5,6,§]

[1]*CAS Key Laboratory of Theoretical Physics, Institute of Theoretical Physics, Chinese Academy of Sciences, Beijing 100190, China*
[2]*School of Physical Sciences, University of Chinese Academy of Sciences, Beijing 100049, China*
[3]*School of Fundamental Physics and Mathematical Sciences, Hangzhou Institute for Advanced Study, University of Chinese Academy of Sciences, Hangzhou 310024, China*
[4]*Peng Huanwu Collaborative Center for Research and Education, Beihang University, Beijing 100191, China*
[5]*Center for Theoretical Physics, Hainan University, Haikou 570228, China*
[6]*Center for Gravitation and Cosmology, College of Physical Science and Technology, Yangzhou University, Yangzhou 225009, China*

(Received 23 January 2024; accepted 3 May 2024; published 29 May 2024)

Understanding the interface dynamics in nonequilibrium quantum systems remains a challenge. We study the interface dynamics of strongly coupled immiscible binary superfluids by using holographic duality. The full nonlinear evolution of the binary superfluids with a relative velocity shows rich nonlinear patterns toward quantum turbulence, which is reminiscent of the quantum Kelvin-Helmholtz instability. The wave number of the fastest growing modes k_0 extracted from the interface pattern yields a nonmonotonic dependence of the relative velocity, independent of the temperature and interaction. The value of k_0 first increases with the velocity difference and then decreases, which stands in sharp contrast to the results of mean-field theory described by the Gross-Pitaevskii equation and is confirmed by using the linear analyses on top of the stationary configuration. We uncover that the critical velocity associated with the maximum corresponds to the case when the mean separation of vortices generated by interface instabilities becomes comparable to the vortex size, which could be a universal physical mechanism at strongly interacting superfluids and is directly testable in laboratory experiments.

DOI: 10.1103/PhysRevD.109.106022

I. INTRODUCTION

Interface instabilities are ubiquitous and are of fundamental interest in fluid dynamics, biological systems, and engineering applications. A well-known one in classical fluid mechanics is Kelvin-Helmholtz instability (KHI) that occurs when there is relative velocity in a single continuous fluid or a velocity difference across the interface between two fluids. This instability, in turn, produces waves, which typically leads to roll-up patterns in the nonlinear stage. Typical examples include the cloud formations on Earth and the Red Spot on Jupiter. There have been growing interests in KHI in quantum fluids. The quantum KHI could play crucial roles in many important phenomena, ranging from the laboratory to astronomical scales, e.g., the pulsar glitches of rotating neutron stars and the vortex formation in atomic Bose-Einstein condensates (BECs). Owing to the quantum characteristics of quantum fluids (e.g., vortex quantization), quantum KHI yields novel nonlinear dynamics that have not been well understood. An ideal testing ground for quantum KHI is superfluids characterized by the vanishing small viscosity. The first experimental observation of quantum KHI was made in [1,2]. It was found that in the presence of shear flow between the A and B phases of superfluid ^{3}He in a rotating cryostat, vortices penetrate from the A phase into the B phase due to KHI. Another natural candidate to study the quantum KHI is the two components BEC which now can be produced in laboratory [3–6].

Various studies related to the quantum KHI have appeared in the literature both experimentally and theoretically [1,2,7–12]. Dynamical instabilities at the interface between two BECs moving relative to each other were investigated using effective theories in the absence of dissipation [11]. The wave number of the most unstable mode $k_0 \sim v^2$ for small velocity difference v, which is reminiscent of classical KHI, while $k_0 \sim v$ for large v, where counterflow instability dominates. After adding dissipation phenomenologically, Landau instability caused by excitation of negative energies occurs in addition [8]. Besides,

*anyuping@itp.ac.cn
†liliphy@itp.ac.cn
‡chuanyinxia@foxmail.com
§hbzeng@yzu.edu.cn

by controlling the relative velocity and the coupling strength between the two components, various patterns can develop [12].

Nevertheless, most of these efforts rely on the Gross-Pitaevskii equation (GPE) which is a model equation for the ground-state single-particle wave function in a weakly interacting BEC. In reality, intraspecies of the superfluids might be strongly coupled, and finite temperature effects and dissipation should also be accounted for. Holography offers us a natural tool to include all those ingredients. The strongly coupled quantum many-body systems at finite temperature and dissipation are encoded to gravitational systems of black holes with one higher dimension. Holographic superfluids have been widely studied in the literature, such as superfluid turbulence [13,14], dark solitons [15], and the Kibble-Zurek mechanism [16–18]. The comparison between holographic superfluids and GPE [19–21] was made as efforts to connect holographic predictions with experiments. Moreover, thus far there are few investigations on the interface dynamics for holographic superfluids.

In this work, we study the interface dynamics of binary strongly coupled superfluids using holography. The stationary patterns obtained from our holographic model share some similarities with GPE. Nevertheless, we focus on the temperature effect on the interface dynamical instabilities far from equilibrium and uncover distinct behavior from GPE [11]. Our investigation unveils a remarkable phenomenon: the most unstable mode k_0 is nonmonotonic as the velocity difference v increases, irrespective of temperature. It first increases, arrives at a maximum, and then decreases as v is increased. Interestingly, we find that the peak location corresponds to the critical case when the average distance of quantized vortices generated along the interface is comparable to the characteristic vortex size. This not only provides a smoking gun for the difference between holography and GPE, but also uncovers a novel underlying mechanism responsible for interface dynamics in strong coupling regime. We now discuss in more detail how we arrive at these results.

II. HOLOGRAPHIC MODEL

We consider a $(3+1)$-dimension bulk theory that holographically describes the interface dynamics of two-component strongly coupled superfluids in two spatial dimensions:

$$\mathcal{L} = \frac{1}{2\kappa_N^2}\left(R + \frac{6}{L^2}\right) + \sum_{i=1}^{2} -(\mathcal{D}_\mu \Psi_i)^* \mathcal{D}^\mu \Psi_i - m_i^2 |\Psi_1|^2 - \frac{\nu}{2}|\Psi_i|^2|\Psi_2|^2 - \frac{1}{4}F^{\mu\nu}F_{\mu\nu}, \tag{1}$$

with R the Ricci scalar, L the anti–de Sitter (AdS) radius, and $\mathcal{D}_\mu \Psi_i = (\nabla_\mu - ie_i A_\mu)\Psi_i$ $(i = 1, 2)$. It involves two complex scalar field Ψ_i charged under the $U(1)$ gauge field A_μ with its strength $F_{\mu\nu}$; see [22,23] for early studies. There is a direct interaction between the two scalar, mimicking the interaction between two components of superfluid.

Working in the probe limit where the backreaction of the matter fields is neglected, we fix the bulk geometry as the Schwarzschild AdS black hole

$$ds^2 = \frac{L^2}{z^2}(-f(z)dt^2 - 2dtdz + dx^2 + dy^2), \tag{2}$$

where $f(z) = 1 - (z/z_h)^3$ with z_h the location of the event horizon. It corresponds to a heat bath with temperature $T = 3/(4\pi z_h)$ on the boundary system. Without loss of generality, we set $L = 1$ and adopt the radial gauge $A_z = 0$. For simplicity, below we choose $m_1^2 = m_2^2 = -2$, $e_1 = e_2 = 1$. Then, near the AdS boundary $z = 0$, asymptotic expansions for matter fields read as

$$A_\mu = a_\mu + b_\mu z + \cdots, \qquad \Psi_i = \Psi_i^{(s)} z + \Psi_i^{(v)} z^2 + \cdots. \tag{3}$$

From the holographic dictionary, we turn off the leading source term, i.e., $\Psi_i^{(s)} = 0$, and thus $\Psi_i^{(v)}$ corresponds to the superfluid condensate $\mathcal{O}_i$. Moreover, $a_t = \mu$ is the chemical potential and $\boldsymbol{a} = (a_x, a_y)$ are related to the superfluid velocity $\boldsymbol{v}_i \equiv (v_x, v_y)_i = \nabla\theta_i - \boldsymbol{a}$, where θ_i is the phase of the condensation $\mathcal{O}_i$ We have used bold-face letters to denote vectors in boundary spatial directions. In practice, we choose $a_x = a_y = 0$, such that the superfluid velocity is given by $\boldsymbol{v}_i = \nabla\theta_i$ for each component. Throughout the paper we will keep the chemical potential of the system fixed. The system enters a superfluid phase below some critical temperature T_c when the order parameter spontaneously develops a nonzero expectation value, which in the gravitational description corresponds to the scalarization of Ψ.

III. STATIONARY CONFIGURATION

We begin with the stationary state describing an immiscible binary superfluid. Without loss of generality, we suppose that the two superfluid components undergo phase separation and form a straight interface at $x = 0$ together with a relative velocity v_y along the y axis. The corresponding bulk configuration is given by

$$\Psi_i = z\phi_i(z,x)e^{i\Theta_i(z,x,y)}, \qquad A_t = A_t(z,x), \tag{4}$$

together with the gauge choice

$$\partial_z \Theta_i = -\frac{A_t}{f}, \qquad V_{iy}(z,x) \equiv \partial_y \Theta_i - A_y. \tag{5}$$

We have $V_{ix} \equiv \partial_x \Theta_i - A_x = 0$ for the stationary state. The phase θ_i of the condensation $\mathcal{O}_i$ is given by $\Theta_i|_{z=0}$ of (4).

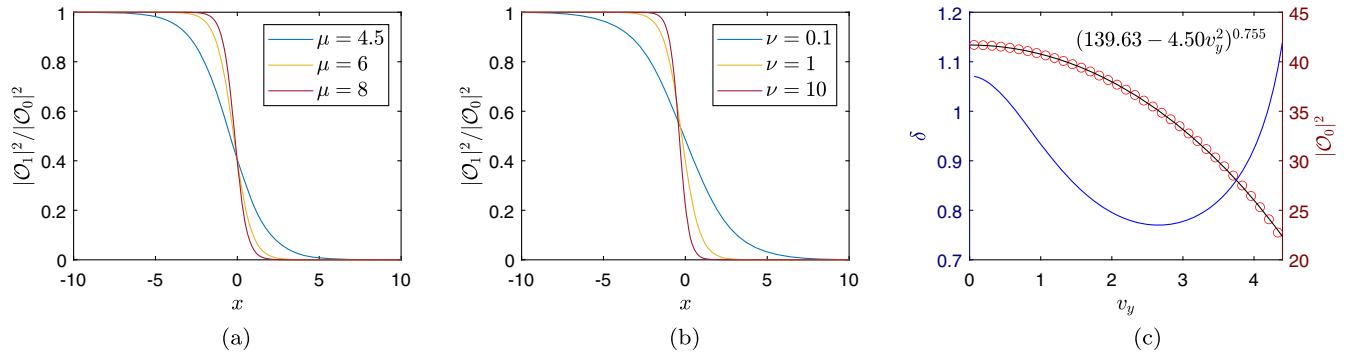

FIG. 1. Stationary configuration for immiscible binary superfluid. The normalized order parameter of the first superfluid component $\mathcal{O}_1$ for different (a) chemical potential μ and (b) coupling ν, with $\mathcal{O}_0$ the value of the order parameter far from the interface. (c) The interface width δ (blue line) and $|\mathcal{O}_0|^2$ (red circles) for different relative velocity v_y. Profiles of $|\mathcal{O}_2|^2$ are mirror image of those of $|\mathcal{O}_1|^2$ about $x = 0$. Black line in (c) is the fitting result. Relavant parameters are (a) $\nu = 1$ and $v_y = 0$, (b) $\mu = 6$ and $v_y = 0$, and (c) $\mu = 6$ and $\nu = 1$.

Note that the phases θ_i depend on the y coordinate because we will consider a relative velocity between the two superfluid components along the y axis. According to the holographic dictionary, one has $V_{1y}|_{z=0} = -V_{2y}|_{z=0} = v_y/2$, where v_y is the relative velocity between the two components. This results in a system of equations of motion involving 5 partial differential equations for (ϕ_i, A_t, V_{iy}) that all depend on the variables z and x. We employ the Newton-Raphson method to solve the system. In the z direction, we use the Chebyshev pseudospectral method, and in the x direction, we adopt the fourth-order finite difference scheme and the Neumann boundary condition.

The normalized profiles of $|\mathcal{O}_1|^2$ for different μ and ν with $v_y = 0$ are shown in Figs. 1(a) and 1(b). Profiles of $|\mathcal{O}_2|^2$ are the mirror image of those of $|\mathcal{O}_1|^2$ about $x = 0$. We see generally that the larger μ and ν are, the narrower the interface is. This feature is qualitatively similar to the results from GPE (see [24] for an early study on the effect of ν in holographic superfluid with $\boldsymbol{\nu} = 0$). The profiles can be fitted by

$$|\mathcal{O}_1|^2 = \frac{|\mathcal{O}_0|^2}{2}(1 - \tanh(x/\delta)), \tag{6}$$

with δ the width of the interface and $\mathcal{O}_0$ the value of the condensation far from the interface. In GPE, when the coupling strength Δ between the two components is small, δ is given by $\delta = \xi/\Delta^{1/2}$ [7], where $\xi = \hbar/\sqrt{2m\mu}$ is the healing length. We have verified numerically that $\delta \sim (\mu - \mu_c)^{-1/2}$ and $\delta \sim \nu^{-1/2}$ when the coupling strength ν is small, which is reminiscent of the result from GPE. In contrast, when the relative velocity is turned on, different behaviors from those of GPE appear, although the shape of condensate can still be fitted by (6). As visible from Fig. 1(c), δ first decreases and then increases with v_y. Such behavior does not show in GPE. Besides, $|\mathcal{O}_0|^2$ versus v_y can be fitted by $|\mathcal{O}_0|^2 = (139.63 - 4.50v_y^2)^{0.755}$, which also significantly deviates from the quadratic speed dependence from GPE. Nevertheless, the value of the power depends on the temperature, but is insensitive to the coupling ν.

IV. DYNAMICAL INTERFACE INSTABILITY

We now provide the numerical simulations of the real-time dynamics. To initiate the dynamical instability, we give a small random noise to the initial stationary condensates. The system size (L_x, L_y) is prepared properly for each parameter set such that the influence of numerical boundaries can be omitted. Please refer to Appendix A for numerical details.

A representative example for the interface dynamics is shown in Fig. 2. Far-from-equilibrium dynamics that are reminiscent of quantum KHI are manifest, just like what happens to the two-component superfluid interface under perturbations from solving GPE [8,11,12]. The amplitude of the sinusoidal interface wave is monotonically increased due to the exponential growth of initial perturbations. The subsequent nonlinear evolution exhibits a quite different behavior from that of the classical fluid. In particular, the interface eventually disintegrates into bubblelike domains of the condensates. As visible from the phase profile θ_1 of the first component, each bubblelike domain contains a quantized vortex (see the bottom panel at $t = 400$). Similar dynamics can be found for different temperatures and relative velocities.

To gain the quantitative feature of the system, we consider the wave number of the most unstable modes k_0 versus the relative velocity v_y. This can be measured directly from experiments. To obtain the mode k_0 that blows up most rapidly, we extract a Fourier spectrum of the shape of interface at each time before the vortices develop. For each v_y, we find a stable peak in Fourier spectrum at k_0 during nonlinear evolution. In practice, for each velocity we run 60

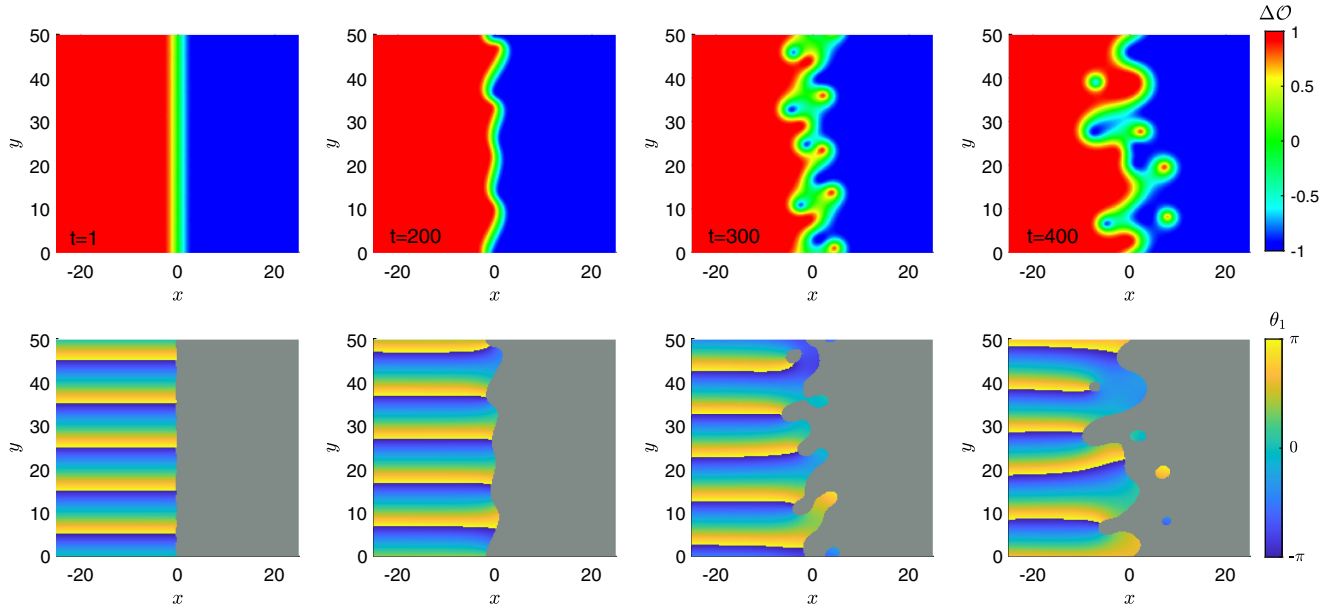

FIG. 2. Interface dynamics for $v_y = 1.2566$ at $T/T_c = 0.677$. Snaps of condensation difference $\Delta\mathcal{O} = (|\mathcal{O}_1|^2 - |\mathcal{O}_2|^2)/|\mathcal{O}_0|^2$ (upper panel) and the profile of the phase of the first component θ_1 (bottom panel) for different time are presented. Small initial perturbations on the interface destabilize and grow into larger amplitude structures leading to vortex formation and quantum turbulence. θ_1 is only plotted for $|\mathcal{O}_1|^2 - |\mathcal{O}_2|^2 > 0$ since otherwise $|\mathcal{O}_1|$ is small and θ_1 would be pure noise. We choose $\nu = 1$ and fix $\mu = 6$.

simulations with different perturbations and compute the mean value of k_0. The results are denoted by the red circles with error bar in Fig. 3(a). Surprisingly, one finds that there is a turning point (denoted as star) for the $k_0 - v_y$ curve.

The onset of the instability can be uncovered from linear response analysis around the stationary state with an interface layer (see Fig. 1) by calculating the quasinormal modes (QNMs); see Appendix B for more details. Since the stationary solution possesses the time translation symmetry and translation symmetry along the y direction, one decomposes small perturbations in terms of Fourier modes $e^{-i(\omega t - ky)}$ where ω and k represent the frequency and wave

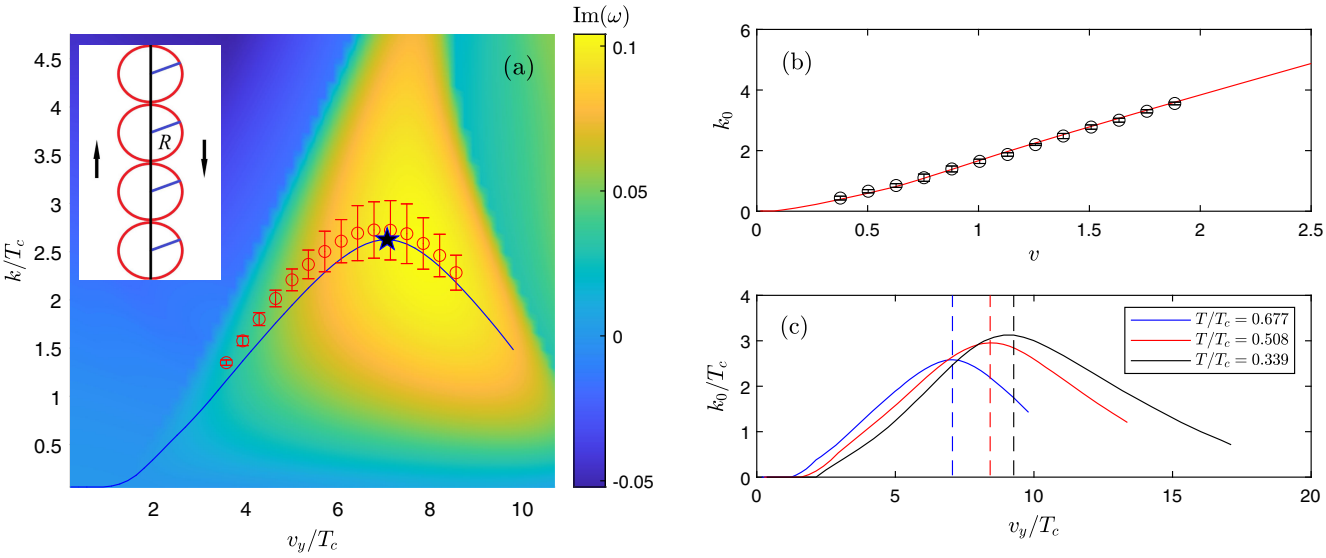

FIG. 3. (a) The wave number of the fastest growing mode k_0 versus the interfacial relative velocity for $T/T_c = 0.677$. The circles with error bar denote k_0 extracted from real time evolution and the solid line from perturbation analysis around the stationary state. The density plot gives the dominant QNMs for each wave number and velocity. Insert illustrates the highest point (star) at which the average distance of vortices $4\pi/v_y$ is equal to the vortex diameter $2R$. (b) $k_0 - v$ relation of GPE at zero temperature. (c) The relation from our holographic theory (1) at different temperatures. Dash vertical lines show the critical velocities by equating the average distance of vortices generated along the interface and the vortex size. We choose $\nu = 1$.

number of the interface wave, respectively. The quasinormal frequencies generically take a complex value due to dissipations into the normal component. Once the imaginary part $\mathrm{Im}(\omega) > 0$, the background becomes dynamically unstable. The wave number of the fastest growing mode corresponds a positive $\mathrm{Im}(\omega)$ that takes a maximum at $k = k_0$. As shown by the density plot of $\mathrm{Im}(\omega)$ in Fig. 3(a), for a given v_y, the imaginary part rises with the increase of k and peaks at a certain wave number that corresponds to the fastest growing mode (see also Fig. 4 in Appendix B). The velocity dependence of the wave number from such dominant QNMs is denoted by the solid blue curve in Fig. 3(a). One can see that the linear analysis agrees quantitatively with the one extracted from fully dynamical evolution. The slight deviation may be due to the relative wide instability spectrum and late-time nonlinear effects.

To compare, we do the same analysis by solving GPE (see Appendix C for more details). The results are shown in Fig. 3(b), from which $k_0 \sim v^2$ for small v and $k_0 \sim v$ for large v. This behavior is in sharp contrast to our holographic results of Fig. 3(a). Another difference is that holographic simulation yields quite small k_0 in the small velocity regime. A possible reason might be that no dissipation and temperature effect are considered in GPE.

A heuristic picture for the nonmonotonic behavior in Fig. 3(a) is given as follows. Thanks to the quantum nature of superfluids, in particular the vortex quantization, the number of vortex formation along the interface is approximately given by $N = \frac{\Delta\theta}{2\pi} = \frac{v_y L_y}{4\pi}$ for our present system. Therefore, the average distance of vortices along the interface is estimated statistically as $L_0 = L_y/N = 4\pi/v_y$. Meanwhile, it is anticipated to create more vortices for a large wave number of the interface instability [25]. On the other hand, the vortex size can be obtained from the static vortex configuration which is axisymmetric, and the condensation depends only on the radial coordinate (see, e.g., [26]). As v_y is increased, the average distance of vortices L_0 will decrease. At a critical velocity $v_c = 2\pi/R$ for which $L_0 = 2R$ with R the radius of a vortex, the vortices near the interface become so dense that they make immediate contact with each other; see insert of Fig. 3(a) for an illustration. The nonlinear vortex dynamics becomes important and prevents the increase of more vortices from the interface instability. Therefore, the corresponding value of the fastest growing mode k_0 at v_c is the maximal wave number among all unstable modes. The above heuristic analysis agrees quantitatively with our numerical computations. Defining the radius of a single vortex R at which $|\mathcal{O}(R)|^2/|\mathcal{O}_0|^2 = 0.98$, we get $v_c/T_c = 2\pi/(RT_c) = 7.06$ for $T/T_c = 0.677$, matching exactly with the turning point in Fig. 3(a). This is also confirmed for other temperatures; see Fig. 3(c). Notice that the value of v_y associated with the turning point does not correspond to the one for δ depicted e.g. in Fig. 1(c). We highlight that the velocity range shown in Fig. 3 is below the critical velocity given by the Landau criterion, and thus our interface dynamics is not due to the Landau instability [27–30]. To have a better understanding of the interface instabilities, it will be helpful to work out the thermodynamics of a binary superfluid. Exploring the thermodynamics of inhomogenous binary superfluids and the thermodynamic instabilities is challenging and lies beyond the scope of our present investigation.

V. DISCUSSION

In this work, we study the interface dynamics of two-component superfluids at strong coupling. The interface separating the two phases of superfluid becomes unstable as the relative velocity is increased. The pattern observed from fully nonlinear simulation is reminiscent of quantum KHI. From both the far-from-equilibrium evolution and the linear QNMs analysis, we find that the wave number of the most unstable modes depends nonmonotonically on the superfluid velocity, in sharp contrast to the results of GPE. We have uncovered that the turning point occurs when the mean separation of vortices generated by interface instabilities becomes comparable to the size of vortices, suggesting that the nonmonotonicity is due to the direct interaction between neighbor vortices. Moreover, as visible from Figs. 3(a) and 3(c), the instability develops noticeably only above a threshold value, which might be due to the dissipation and viscous effect away from the ground state. These findings are directly testable in platform, like strongly coupled ultracold Bose gases or thin helium films at low temperatures.

Our study broadens the application of holography to nonequilibrium phenomena with finite temperature and dissipation. In particular, it initiates the investigation of interface instabilities in the holography laboratory, providing an intriguing platform to explore the interplay of instabilities and the emergence of complex flow phenomena. There are several lines of research in which our study can be extended, shedding light on the complicated behaviors of interface dynamics. For example, owing to the relative velocity between superfluid component and normal component, one anticipates that the interface of binary superfluids that move with the same velocity relative to the normal component can be unstable at finite temperature [1]. Since GPE is at zero temperature, this phenomenon cannot be presented from GPE. In contrast, the temperature effect is naturally incorporated in our holographic model, and, indeed, this is the case and will be reported elsewhere. Moreover, quantized vortices with a higher winding number can develop [31], which could complicate the interface dynamics. The turbulent dynamical behavior is anticipated following closely the initial emission of vortex-antivortex pairs. Moreover, the introduction of external magnetic field and rotation is of interest.

ACKNOWLEDGMENTS

We thank Fanlong Meng, Tao Shi, Hongbao Zhang, and Yu Tian for useful comments and suggestions. This work is partly supported by the National Natural Science Foundation of China No. 12122513, No. 12075298, and No. 12275233. We acknowledge the use of the High Performance Cluster at Institute of Theoretical Physics, Chinese Academy of Science.

APPENDIX A: NUMERICAL SCHEME OF THE FULLY NONLINEAR SIMULATIONS

Here we provide additional technical details on the derivation of the main results reported in the main text.

The general equations of motion for our matter fields read as

$$\mathcal{D}_\mu \mathcal{D}^\mu \Psi_i - m_i^2 \Psi_i - \frac{\nu}{2}|\Psi_j|^2 \Psi_i = 0, \quad (i,j=1,2 \;\; i \neq j), \tag{A1}$$

$$\nabla_\mu F^{\mu\nu} = -2\mathrm{Im}\left(\sum_i \Psi_i^* \mathcal{D}^\nu \Psi_i\right), \tag{A2}$$

where Im represents imaginary part. The bulk equations of motion on top of the background (2) are explicitly given by

$$2\partial_t\partial_z\Phi_i - \Big[2iA_t\partial_z\Phi_i + i\partial_z A_t\Phi_i + \partial_z(f\partial_z\Phi_i) - z\Phi_i + \partial_x^2\Phi_i + \partial_y^2\Phi_i - i(\partial_x A_x + \partial_y A_y)\Phi_i - (A_x^2 + A_y^2)\Phi_i - 2i(A_x\partial_x\Phi_i + A_y\partial_y\Phi_i) - \frac{\nu}{2}|\Phi_j|^2\Phi_i\Big] = 0, \quad (i,j=1,2 \quad i \neq j) \tag{A3}$$

$$\partial_t\partial_z A_t - \Big[\partial_x^2 A_t + \partial_y^2 A_t + f\partial_z(\partial_x A_x + \partial_y A_y) - \partial_t(\partial_x A_x + \partial_y A_y) - 2A_t\sum_i |\Phi_i|^2 - 2f\mathrm{Im}\left(\sum_i \Phi_i^*\partial_z\Phi_i\right) + 2\mathrm{Im}\left(\sum_i \Phi_i^*\partial_t\Phi_i\right)\Big] = 0, \tag{A4}$$

$$2\partial_t\partial_z A_x - \left[\partial_z(\partial_x A_t + f\partial_z A_x) + \partial_y(\partial_y A_x - \partial_x A_y) - 2A_x\sum_i |\Phi_i|^2 + 2\mathrm{Im}\left(\sum_i \Phi_i^*\partial_x\Phi_i\right)\right] = 0, \tag{A5}$$

$$2\partial_t\partial_z A_y - \left[\partial_z(\partial_y A_t + f\partial_z A_y) + \partial_x(\partial_x A_y - \partial_y A_x) - 2A_y\sum_i |\Phi_i|^2 + 2\mathrm{Im}\left(\sum_i \Phi_i^*\partial_y\Phi_i\right)\right] = 0, \tag{A6}$$

$$\partial_z(\partial_x A_x + \partial_y A_y - \partial_z A_t) - 2\mathrm{Im}\left(\sum_i \Phi_i^*\partial_z\Phi_i\right) = 0, \tag{A7}$$

where $\Phi_i = \Psi_i/z$. For simplicity, we have chosen $m_1^2 = m_2^2 = -2/L^3$, $e_1 = e_2 = L = 1$ and have adopted the radial gauge $A_z = 0$. Notice the last equation is a constraint with no time derivative. These equations are not independent. They obey the following constraint equation:

$$-\partial_t \mathrm{Eq.}\ (Constraint) - \partial_z \mathrm{Eq.}\ (A_t) + \partial_x \mathrm{Eq.}\ (A_x) + \partial_y \mathrm{Eq.}\ (A_y) = 2\mathrm{Im}\left(\sum_i \mathrm{Eq.}\ (\Phi_i) \times \Phi_{0i}^*\right). \tag{A8}$$

where Eq. (Φ_i), Eq.(A_t), Eq.(A_x), Eq.(A_y), Eq.(Constraint) correspond to Eq. (A3)–(A7).

The expansions of the fields near the AdS boundary $z = 0$ can be obtained as

$$A_\mu = a_\mu + b_\mu z + \cdots, \qquad \Phi_i = (\Phi_i)_s + (\Phi_i)_v z + \cdots. \tag{A9}$$

From the holographic duality, the coefficients a_t, a_i $(i = x,\ y)$ and $(\Phi_i)_0$ are interpreted as the chemical potential μ, vector potential, and scalar operator source of the boundary theory, respectively. To describe superfluid where the U(1) symmetry is broken spontaneously, we should turn off the scalar source, i.e., $(\Phi_i)_s = 0$. Then the superfluid condensation is given as $\mathcal{O}_i = (\Psi_i)_v$ in the standard quantization.

Note that T and μ are not independent quantities because of scaling symmetry of the system. After fixing $z_h = 1$, μ is the only free parameter. Then, there is a second order phase transition for our present setup when $\mu \geq \mu_c \simeq 4.064$. This also fixes the ratio $T/T_c = \mu_c/\mu$. In practice, we fix $T = 3/4\pi$, so $T_c = \mu T/\mu_c$ should depend on μ.

The fully nonlinear simulation starts with the initial data

$$\Phi = \Phi_{i0} + \delta\Phi_i, \qquad A_\mu = A_{\mu 0} + \delta A_\mu, \tag{A10}$$

where Φ_{i0} and $A_{\mu 0}$ denote the corresponding profile for the stationary interface configuration (see, e.g., Fig. 1 in the main text). For simplicity but without loss of generality, we use a sum of evenly distributed modes as the initial condition:

$$\delta\Phi_i = (-1)^{i-1}\sum_k z\exp(-x^2)\exp(iky + i\theta_k)\exp(i(v_i)_y),$$
$$\delta A_\mu = 0, \tag{A11}$$

where θ_k is a random phase for each wave number k.

Our evolution scheme is implemented numerically by the fourth order Runge-Kutta method along the time direction. Moreover, we use the Chebyshev pseudospectral method along the z direction and Fourier pseudospectral method along the y coordinate. To capture the dynamics near the interface, we adopt the fourth order finite difference scheme in the x direction. Previous holographic investigations deal exclusively with the periodic boundary condition along the x direction and therefore cannot properly accommodate the interface dynamics.

First, we use (A3), (A5), and (A6) to evolve Φ, A_x, and A_y subject to the source free boundary condition at the AdS boundary:

$$\Phi(z=0) = A_x(z=0) = A_y(z=0) = 0, \tag{A12}$$

together with the Neumann boundary condition

$$\partial_x\Phi = \partial_x A_\mu = 0, \tag{A13}$$

at $x = \pm L_x/2$, where the system size L_x is prepared properly for each parameter set such that the influence of numerical boundaries can be omitted. Note that the boundary condition has been implicitly adopted in our numerical computation.

Then we use (A4) to evolve $\partial_z A_t$ on the AdS boundary. Since we set the chemical potential μ as a constant, $-\partial_z A_t(z=0)$ is just the charge density ρ of the dual boundary system. Finally, A_t can be solved by the constraint equation (A7) subject to the boundary condition

$$\partial_z A_t(z=0) = -\rho, \qquad A_t(z=0) = \mu. \tag{A14}$$

The later time configuration can be obtained in the same way as described before.

APPENDIX B: LINEAR INSTABILITY AROUND A STATIONARY CONFIGURATION

The onset of the instability of such stationary solutions can be analyzed by the linear response theory. To be more specific, we turn to the linear perturbations on the stationary background,

$$\Phi_i = \Phi_{i0} + \delta\Phi_i, \qquad A_t = A_{t0} + \delta A_t,$$
$$A_x = A_{x0} + \delta A_x, \qquad A_y = A_{y0} + \delta A_y, \tag{B1}$$

where Φ_{0i}, A_{t0}, A_{x0}, and A_{y0} are stationary solutions as shown in Fig. 1 in the main text. Taking into account the translation invariance of our background along the time and y directions, as well as the velocity difference across the interface between two superfluids, one takes the bulk perturbation fields as the form of

$$\delta\Phi_i = u_i(z,x)e^{-i(\omega t - ky)}e^{i(v_i)_y y}, \qquad \delta\Phi_i^* = v_i(z,x)e^{-i(\omega t-ky)}e^{-i(v_i)_y y},$$
$$\delta A_t = a_t(z,x)e^{-i(\omega t-ky)}, \qquad \delta A_x = a_x(z,x)e^{-i(\omega t-ky)}, \qquad \delta A_y = a_y(z,x)e^{-i(\omega t-ky)}, \tag{B2}$$

where $(v_1)_y = -(v_2)_y = v_y/2$ with v_y the relative velocity between the two superfluid components. The resulting linear perturbation equations are given explicitly as

$$
\begin{aligned}
&2iA_{t0}\partial_z u_i + 2ia_t\partial_z\Phi_{0i} + i\partial_z A_{t0}u_i + i\partial_z a_t\Phi_{0i} + \partial_z(f\partial_z u_i) - zu_i + \partial_x^2 u_i - (k+(v_i)_y)^2 u_i - i\partial_x A_{x0}u_i \\
&\quad - i\Phi_{0i}(\partial_x a_x + ika_y) - (A_{x0}^2 + A_{y0}^2)u_i - 2A_{x0}\Phi_{0i}a_x - 2A_{y0}\Phi_{0i}a_y - 2i(A_{x0}\partial_x u_i + i(k+(v_i)_y)A_{y0}u_i) \\
&\quad - 2i(a_x\partial_x\Phi_{0i} + ia_y(v_i)_y\Phi_{0i}) - \frac{\nu}{2}|\Phi_{0j}|^2 u_i - \frac{\nu}{2}\Phi_{0j}^*\Phi_{0i}u_j - \frac{\nu}{2}\Phi_{0j}\Phi_{0i}v_j \\
&= -2i\omega\partial_z u_i, \quad (i,j=1,2 \quad i\neq j), \\
&\quad - 2iA_{t0}\partial_z v_i - 2ia_t\partial_z\Phi_{0i}^* - i\partial_z A_{t0}v_i - i\partial_z a_t\Phi_{0i}^* + \partial_z(f\partial_z v_i) - zv_i + \partial_x^2 v_i - (k-(v_i)_y)^2 v_i + i\partial_x A_{x0}v_i \\
&\quad + i\Phi_{0i}^*(\partial_x a_x + ika_y) - (A_{x0}^2 + A_{y0}^2)v_i - 2A_{x0}\Phi_{0i}^* a_x - 2A_{y0}\Phi_{0i}^* a_y + 2i(A_{x0}\partial_x v_i + i(k-(v_i)_y)A_{y0}v_i) \\
&\quad + 2i(a_x\partial_x\Phi_{0i}^* - ia_y(v_i)_y\Phi_{0i}^*) - \frac{\nu}{2}|\Phi_{0j}|^2 v_i - \frac{\nu}{2}\Phi_{0j}\Phi_{0i}^* v_j - \frac{\nu}{2}\Phi_{0j}^*\Phi_{0i}^* u_j \\
&= -2i\omega\partial_z v_i, \quad (i,j=1,2 \quad i\neq j), \\
&\quad \partial_x^2 a_t - k^2 a_t + f\partial_z\partial_x a_x + ikf\partial_z a_y - 2a_t\sum_i|\Phi_{0i}|^2 - 2A_{t0}\sum_i(\Phi_{0i}^* u_i + \Phi_{0i}v_i) + if\sum_i(\Phi_{0i}^*\partial_z u_i \\
&\quad - \Phi_{0i}\partial_z v_i + v_i\partial_z\Phi_{0i} - u_i\partial_z\Phi_{0i}^*) = -i\omega(\partial_z a_t + \partial_x a_x + ika_y) + \omega\sum_i(\Phi_{0i}^* u_i - \Phi_{0i}v_i), \\
&\quad \partial_z(\partial_x a_t + f\partial_z a_x) - (k^2 a_x + ik\partial_x a_y) - 2a_x\sum_i|\Phi_{0i}|^2 - 2A_{x0}\sum_i(\Phi_{0i}^* u_i + \Phi_{0i}v_i) \\
&\quad - i\sum_i(\Phi_{0i}^*\partial_x u_i - \Phi_{0i}\partial_x v_i + v_i\partial_x\Phi_{0i} - u_i\partial_x\Phi_{0i}^*) = -2i\omega\partial_z a_x, \\
&\quad ik\partial_z a_t + \partial_z(f\partial_z a_y) + \partial_x^2 a_y - ik\partial_x a_x - 2a_y\sum_i|\Phi_{0i}|^2 - 2A_{y0}\sum_i(\Phi_{0i}^* u_i + \Phi_{0i}v_i) \\
&\quad + \sum_i((k+(v_i)_y)\Phi_{0i}^* u_i - (k-(v_i)_y)\Phi_{0i}v_i + (v_i)_y v_i\Phi_{0i} + (v_i)_y u_i\Phi_{0i}^*) = -2i\omega\partial_z a_y. \qquad \text{(B3)}
\end{aligned}
$$

For more stable numerical performance, we use the following equation for a_t:

$$
\begin{aligned}
&\partial_z(\partial_x a_x + ika_y - \partial_z a_t) + i\sum_i(\Phi_i^*\partial_z u_i + v_i\partial_z\Phi_i \\
&\quad - u_i\partial_z\Phi_i^* - \Phi_i\partial_z v_i) = 0, \qquad \text{(B4)}
\end{aligned}
$$

which comes from the constraint equation (A7). Moreover, we require the last perturbation equation of (B3) to be satisfied at the AdS boundary $z=0$, yielding

$$
(\partial_z\partial_x a_x + ik\partial_z a_y = -i\omega\partial_z a_z)|_{z=0}. \qquad \text{(B5)}
$$

Then, by considering (A8), the last perturbation equation is also satisfied in the whole bulk. Regarding other perturbed fields, we impose the source free boundary condition at the AdS boundary. We further consider the Neumann boundary condition at $x=\pm L_x/2$.

The corresponding quasinormal modes are extracted by solving the above generalized eigenvalue problem. Then we can numerically obtain ω for each k and velocity difference v_y. Owing to dissipations into the normal component, the quasinormal frequencies generically take a complex value. Since $\delta\Phi_i \sim e^{-i\omega t}$, the stationary configuration will become dynamically unstable whenever $\mathrm{Im}(\omega) > 0$. The larger the positive imaginary part is, the more unstable the system becomes. In Fig. 4, we demonstrate the spectrum of QMNs versus k for $v_y = 3.5132$ at $T/T_c = 0.677$ and $\nu = 1$. The imaginary part rises with the increase of k and peaks at a certain wave number that corresponds to the fastest growing mode. The case for the linear perturbation analysis of GPE is exactly the same, but much simpler.

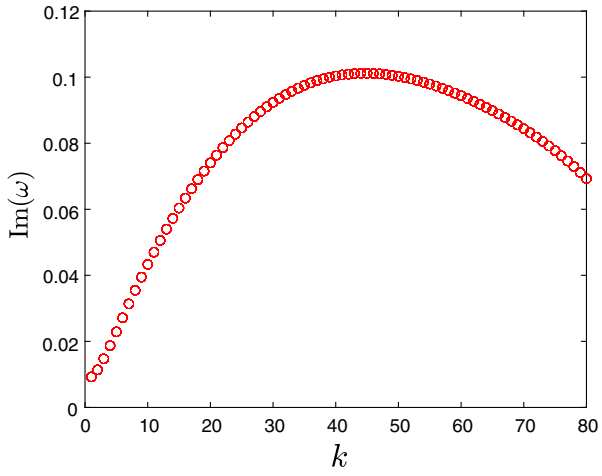

FIG. 4. The imaginary low lying spectrum of QNMs of stationary configurations with $T/T_c = 0.677$ and $v_y = 2.5132$. The peak of $\mathrm{Im}(\omega)$ determines the wave number of the fastest growing mode. We fix $\nu = 1$ and $\mu = 6$.

APPENDIX C: INTERFACE INSTABILITY FROM GPE

Two-component superfluids can be described by following coupled GPEs [32]:

$$i\partial_t\Psi_i = \left(-\frac{1}{2m_i}\nabla^2 - \mu_i + g_i|\Psi_i|^2 + g_{ij}|\Psi_j|^2 + V_i\right)\Psi_i, \quad (i,j=1,2, \quad i\neq j). \tag{C1}$$

Here we focus on $g_{12} > \sqrt{g_1 g_2}$, which gives immiscible BECs, and we also set $V_i = 0$. To study two-component superfluids with interface and relative velocity, we use the ansatz

$$\Psi_i(\mathbf{r}) = \psi_i(x)e^{im_i v_i y}, \tag{C2}$$

with $v_1 = -v_2 = v$. Substituting (C2) into (C1), we get the following time-independent GPE for $\psi_i(x)$:

$$\left(-\frac{1}{2m_i}\partial_x^2 - \mu_i + \frac{m_i v^2}{2} + g_i|\psi_i|^2 + g_{ij}|\psi_j|^2\right)\psi_i = 0, \quad (i,j=1,2, \quad i\neq j). \tag{C3}$$

Far from the interface, we have $\partial_y\psi_i = 0$, $\psi_j = 0$, and therefore $\psi_i = (\mu_i - m_i v^2/2)/g_i = \sqrt{n_i}$. Profiles for ψ_i solved from these equations are similar to those shown in Fig. 1.

Next let us study the interface instability using linear perturbation analysis. Adding perturbations on the stationary background ψ_i^0

$$\Psi_i = \left[\psi_i^0(x) + u_i(x)e^{iky - i\omega t} - w_i^*(x)e^{-iky + i\omega^* t}\right]e^{im_i v_i y}, \tag{C4}$$

and linearizing GPEs, we obtain the Bogoliubov-de Gennes (BdG) equation

$$\mathcal{H}\mathbf{U} = \omega\mathbf{U}, \tag{C5}$$

$$\mathcal{H} = \begin{Bmatrix} h_1^+ & -g_1(\psi_1^0)^2 & g_{12}\psi_1^0\psi_2^0 & -g_{12}\psi_1^0\psi_2^0 \\ g_1(\psi_1^0)^2 & -h_1^- & g_{12}\psi_1^0\psi_2^0 & -g_{12}\psi_1^0\psi_2^0 \\ g_{12}\psi_1^0\psi_2^0 & -g_{12}\psi_1^0\psi_2^0 & h_2^+ & -g_2(\psi_2^0)^2 \\ g_{12}\psi_1^0\psi_2^0 & -g_{12}\psi_1^0\psi_2^0 & g_2(\psi_2^0)^2 & -h_2^- \end{Bmatrix}, \tag{C6}$$

with $\mathbf{U} = (u_1, w_1, u_2, w_2)^{\mathrm{T}}$ and

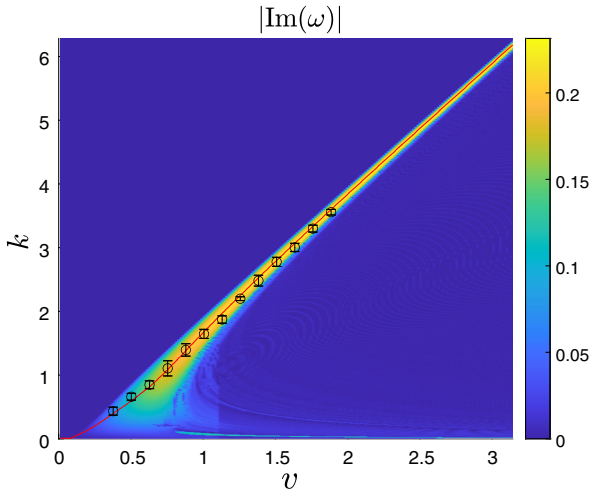

FIG. 5. The wave number of the fastest growing mode versus the superflow velocity $v_1 = -v_2 = v$ obtained from GPEs. The red solid line is from perturbation analysis of (C5), and the black circles with error bars are extracted from dynamical evolution. The density plot shows the dominant $|\mathrm{Im}(\omega)|$ for each wave number and velocity. We have chosen $g = m = 1$, $g_{12} = 2$, and $\mu = 0.5$.

$$h_i^{\pm} = -\frac{1}{2m_i}[\partial_x^2 - (k \pm m_i v_i)^2] - \mu_i + 2g_i|\psi_i^0|^2 + g_{ij}|\psi_j^0|^2. \tag{C7}$$

By numerically diagonalizing this discretized BdG equation Hamiltonian $\mathcal{H}$, we can get the eigenfrequency ω. Since this Hamiltonian $\mathcal{H}$ is real, we also have $\mathcal{H}\mathbf{U}^* = \omega^*\mathbf{U}^*$, i.e., ω^* is also an eigenvalue whenever ω is an eigenvalue. Therefore, whenever $\mathrm{Im}(\omega) \neq 0$, the system is dynamically unstable. For convenience, we set $g_{12} = 2$, $g_1 = g_2 = 1$, $m_1 = m_2 = 1$, and $\mu_1 - m_1 v_1^2/2 = \mu_2 - m_2 v_2^2/2 = \mu = 0.5$ when doing numerical calculations.

By calculating $\mathrm{Im}(\omega)$ for different v and k, we can extract the wave number k_0 of the most unstable mode for each v, which can be compared with the results from our holographic model. We have also done the fully nonlinear time evolution to extract k_0 with the same procedure as in the holographic case. The results are shown in Fig. 5. We see the values of k_0 extracted from both linear analysis and dynamical evolution agree well with each other. From Fig. 5, we also find that $k_0 \sim v^2$ for small v and $k_0 \sim v$ for large v, corresponding to the Kelvin-Helmholtz instability and the countersuperflow instability, respectively, as shown in [11]. This result is qualitatively different from the one from our holographic model (see Fig. 3).

[1] G. E. Volovik, On the Kelvin-Helmholtz instability in superfluids, JETP Lett. **75**, 418 (2002).

[2] R. Blaauwgeers, V. B. Eltsov, G. Eska, A. P. Finne, R. P. Haley, M. Krusius, J. J. Ruohio, L. Skrbek, and G. E. Volovik, Shear flow and Kelvin-Helmholtz instability in superfluids, Phys. Rev. Lett. **89**, 155301 (2002).

[3] S. B. Papp, J. M. Pino, and C. E. Wieman, Tunable miscibility in a dual-species Bose-Einstein condensate, Phys. Rev. Lett. **101**, 040402 (2008).

[4] G. Thalhammer, G. Barontini, L. De Sarlo, J. Catani, F. Minardi, and M. Inguscio, Double species Bose-Einstein condensate with tunable interspecies interactions, Phys. Rev. Lett. **100**, 210402 (2008).

[5] S. Tojo, Y. Taguchi, Y. Masuyama, T. Hayashi, H. Saito, and T. Hirano, Controlling phase separation of binary Bose-Einstein condensates via mixed-spin-channel Feshbach resonance, Phys. Rev. A **82**, 033609 (2010).

[6] D. J. McCarron, H. W. Cho, D. L. Jenkin, M. P. Köppinger, and S. L. Cornish, Dual-species Bose-Einstein condensate of ^{87}Rb and ^{133}Cs, Phys. Rev. A **84**, 011603 (2011).

[7] R. A. Barankov, Boundary of two mixed Bose-Einstein condensates, Phys. Rev. A **66**, 013612 (2002).

[8] H. Takeuchi, N. Suzuki, K. Kasamatsu, H. Saito, and M. Tsubota, Quantum Kelvin-Helmholtz instability in phase-separated two-component Bose-Einstein condensates, Phys. Rev. B **81**, 094517 (2010).

[9] A. P. Finne, V. B. Eltsov, R. Hänninen, N. B. Kopnin, J. Kopu, M. Krusius, M. Tsubota, and G. E. Volovik, Dynamics of vortices and interfaces in superfluid ^{3}He, Rep. Prog. Phys. **69**, 3157 (2006).

[10] V. B. Eltsov, A. Gordeev, and M. Krusius, Kelvin-Helmholtz instability of *ab* interface in superfluid ^{3}He, Phys. Rev. B **99**, 054104 (2019).

[11] N. Suzuki, H. Takeuchi, K. Kasamatsu, M. Tsubota, and H. Saito, Crossover between Kelvin-Helmholtz and counter-superflow instabilities in two-component Bose-Einstein condensates, Phys. Rev. A **82**, 063604 (2010).

[12] H. Kokubo, K. Kasamatsu, and H. Takeuchi, Pattern formation of quantum Kelvin-Helmholtz instability in binary superfluids, Phys. Rev. A **104**, 023312 (2021).

[13] A. Adams, P. M. Chesler, and H. Liu, Holographic vortex liquids and superfluid turbulence, Science **341**, 368 (2013).

[14] Y. Du, C. Niu, Y. Tian, and H. Zhang, Holographic thermal relaxation in superfluid turbulence, J. High Energy Phys. 12 (2015) 018.

[15] M. Guo, E. Keski-Vakkuri, H. Liu, Y. Tian, and H. Zhang, Dynamical phase transition from nonequilibrium dynamics of dark solitons, Phys. Rev. Lett. **124**, 031601 (2020).

[16] P. M. Chesler, A. M. Garcia-Garcia, and H. Liu, Defect formation beyond Kibble-Zurek mechanism and holography, Phys. Rev. X **5**, 021015 (2015).

[17] J. Sonner, A. del Campo, and W. H. Zurek, Universal far-from-equilibrium dynamics of a holographic superconductor, Nat. Commun. **6**, 7406 (2015).

[18] A. del Campo, F. J. Gómez-Ruiz, Z.-H. Li, C.-Y. Xia, H.-B. Zeng, and H.-Q. Zhang, Universal statistics of vortices in a newborn holographic superconductor: Beyond the Kibble-Zurek mechanism, J. High Energy Phys. 06 (2021) 061.

[19] P. Wittmer, C.-M. Schmied, T. Gasenzer, and C. Ewerz, Vortex motion quantifies strong dissipation in a holographic superfluid, Phys. Rev. Lett. **127**, 101601 (2021).

[20] Y.-K. Yan, S. Lan, Y. Tian, P. Yang, S. Yao, and H. Zhang, Holographic dissipation prefers the Landau over the Keldysh form, Phys. Rev. D **107**, L121901 (2023).

[21] W.-C. Yang, C.-Y. Xia, H.-B. Zeng, M. Tsubota, and J. Zaanen, Motion of a superfluid vortex according to holographic quantum dissipation, Phys. Rev. B **107**, 144511 (2023).

[22] P. Basu, J. He, A. Mukherjee, M. Rozali, and H.-H. Shieh, Competing holographic orders, J. High Energy Phys. 10 (2010) 092.

[23] R.-G. Cai, L. Li, L.-F. Li, and Y.-Q. Wang, Competition and coexistence of order parameters in holographic multi-band superconductors, J. High Energy Phys. 09 (2013) 074.

[24] W.-C. Yang, C.-Y. Xia, H.-B. Zeng, and H.-Q. Zhang, Phase separation and exotic vortex phases in a two-species holographic superfluid, Eur. Phys. J. C **81**, 21 (2021).

[25] See the argument in [15]. For the snake instability, it was shown that the unsatble mode with wave number k will create $N = \frac{kL_y}{2\pi}$ pairs of vortices [15].

[26] V. Keranen, E. Keski-Vakkuri, S. Nowling, and K. P. Yogendran, Inhomogeneous structures in holographic superfluids: II. Vortices, Phys. Rev. D **81**, 126012 (2010).

[27] I. Amado, D. Areán, A. Jiménez-Alba, K. Landsteiner, L. Melgar, and I. Salazar Landea, Holographic superfluids and the Landau criterion, J. High Energy Phys. 02 (2014) 063.

[28] S. Lan, H. Liu, Y. Tian, and H. Zhang, Landau instability and soliton formations, arXiv:2010.06232.

[29] B. Goutéraux, E. Mefford, and F. Sottovia, Critical superflows and thermodynamic instabilities in superfluids, Phys. Rev. D **108**, L081903 (2023).

[30] D. Areán, B. Goutéraux, E. Mefford, and F. Sottovia, Hydrodynamics and instabilities of relativistic superfluids at finite superflow, arXiv:2312.08243.

[31] S. Lan, X. Li, Y. Tian, P. Yang, and H. Zhang, Heating up quadruply quantized vortices: Splitting patterns and dynamical transitions, Phys. Rev. Lett. **131**, 221602 (2023).

[32] W. H. Bassichis, Generalization of the Boguliubov method applied to mixtures of Bose-Einstein particles, Phys. Rev. **134**, A543 (1964).